Inorg. Chem. **2002**, *41*, 6838–6845

Synthetic, Structural, Electrochemical, and Theoretical Studies of Heterometallic Aggregates with a $[Pt_2(\mu\text{-}S)_2M]$ Core (M = Hg, Au)

Xingling Xu,[†,‡] S.-W. Audi Fong,[‡] Zhaohui Li,[‡] Zhi-Heng Loh,[‡] Feng Zhao,[‡] Jagadese J. Vittal,[‡] William Henderson,[§] Soo-Beng Khoo,*[,‡] and T. S. Andy Hor*[,‡]

Department of Chemistry, National University of Singapore, 3 Science Drive 3, Singapore 117543, and Department of Chemistry, University of Waikato, Private Bag 3105, Hamilton, New Zealand

Received November 16, 2001

Novel electroactive multimetallic compounds based on the $\{Pt_2(\mu_2\text{-}S)_2M\}$ core, viz. $[Pt_2(PPh_3)_4(\mu_3\text{-}S)_2HgFc]PF_6$ (**1**) [Fc = $(\eta^5\text{-}C_5H_4)Fe(\eta^5\text{-}C_5H_5)$] and $[Pt_2(PPh_3)_4(\mu_3\text{-}S)_2Hg_2Fc']PF_6)_2$ (**2**) [Fc′ = $Fe(\eta^5\text{-}C_5H_4)_2$], have been synthesized under the guide of electrospray mass spectrometry. The electrochemistry of these ferrocene funtionalized compounds together with the reported $[Pt_2(PPh_3)_4(\mu_3\text{-}S)_2HgPPh_3](PF_6)_2$ (**3**), $[Pt_2(PPh_3)_4(\mu_2\text{-}S)(\mu_3\text{-}S)HgPh]PF_6$ (**4**), and $[Pt_2(PPh_3)_4(\mu_2\text{-}S)(\mu_3\text{-}S)AuPPh_3]PF_6$ (**5**) have been investigated using cyclic voltammetry and DFT calculations. These results point to a prominent ligand-based oxidation.

Introduction

Multimetallic compounds with the $\{Pt_2(\mu_2\text{-}S)_2M\}$ core have been extensively investigated in the past decade. In principle, the heterometal M can be any metallic element in the periodic table with a variety of coordination geometries and structures.[1] This universal nature of M, the adaptation of the $\{Pt_2M\}$ core, and its easy preparation from the metalloligand $[Pt_2(PPh_3)_4(\mu_2\text{-}S)_2]$ (**L**) make this an attractive aggregate and cluster system for experimental and theoretical studies. As the platinum center is practically saturated, the dominant features of these aggregates are often determined by the nature and activity of M. To date, we have assembled a large collection of those aggregates with M bearing one (or more) labile ligand(s), which are hence potentially unsaturated, for example, $Pt_2(PPh_3)_4(\mu_3\text{-}S)_2Pb(NO_3)_2$,[2a] $[Pt_3(PPh_3)_2(\mu_3\text{-}S)_2(cod)_2]^{2+}$,[2b] $Pt_2(PPh_3)_4(\mu_3\text{-}S)_2BiCl_2NO_3$,[2c] $[Pt_2(PPh_3)_4(\mu_3\text{-}S)_2Tl]NO_3$,[2d] and so forth. We are particularly interested in the activity that M can bring to the aggregate, especially its electrocatalytic potential. The structural analogy of this basic metalloligand to the protein enzyme core $[Fe_2(\mu\text{-}S)_2]$,[3] which acts as an excellent electron transfer center in biocatalytic processes, provides an additional impetus for this research. The presence of multimetallic and potentially electroactive centers prompted us to investigate the electrochemistry of these polynuclear complexes. Not only does the capping sulfido ligand in this system bring together and support the multimetallic framework, but it could also serve as a communication center for intermetallic electron transfer. Unfortunately, our earlier study on $[Pt_2(PPh_3)_4(\mu_3\text{-}S)_2Tl]PF_6$ and $[Pt_2(dppf)_2(\mu_3\text{-}S)_2Tl]PF_6$ (**Tl**) [dppf = 1,1′-bis(diphenylphosphino)ferrocene] did not reveal any unusual behavior.[4] The cyclic voltammograms (CVs) did not show any identifiable oxidation or reduction processes except for the normal electrochemical behavior of the attached electroactive ferrocenyl center. Our recent work on the Hg(II) compounds such as $[Pt_2(PPh_3)_4(\mu_3\text{-}S)_2HgPPh_3](PF_6)_2$ was more encouraging,[5] in which a proximate reversible peak was found in its solution cyclic voltammogram. As a continued effort in the exploration of the electrochemical behaviors of this system, we have synthesized related compounds of Au(I) and

* To whom correspondence should be addressed. E-mail: andyhor@nus.edu.sg (T.S.A.H.).

† Present address: School of Chemistry, The Queen's University of Belfast, Belfast BT9 5AG, U.K.

‡ National University of Singapore.

§ University of Waikato.

(1) Fong S.-W. A.; Hor, T. S. A. *J. Chem. Soc., Dalton Trans.* **1999**, 639 and references therein.

(2) (a) Zhou, M.; Xu, Y.; Lam, C.-F.; Leung, P.-H.; Koh, L.-L.; Mok, K. F.; Hor, T. S. A. *Inorg. Chem.* **1993**, *32*, 4660. (b) Zhou M.; Xu, Y.; Tan, A.-M.; Leung, P.-H.; Mok, K. F.; Koh, L.-L.; Hor, T. S. A. *Inorg. Chem.* **1995**, *34*, 6425. (c) Zhou, M. S.; Tan, A.-L.; Xu, Y.; Lam, C.-F.; Leung, P.-H.; Mok, K. F.; Koh, L.-L.; Hor, T. S. A. *Polyhedron* **1997**, *16*, 2381. (d) Zhou, M.; Xu, Y.; Koh, L.-L.; Mok, K. F.; Leung, P.-H.; Hor, T. S. A. *Inorg. Chem.* **1993**, *32*, 1875.

(3) Peters, J. W.; *Curr. Opin. Struct. Biol.* **1999**, *9*, 670. Peters, J. W.; Lanzilotta, W. N.; Lemon, B. J.; Seefeldt, L. C. *Science* **1998**, *282*, 1853.

(4) Phang, L.-T.; Au-Yeung, S. C. F.; Hor, T. S. A.; Khoo, S. B.; Zhou, Z.-Y.; Mak, T. C. W. *J. Chem. Soc., Dalton Trans.* **1993**, 165.

(5) Li, Z.; Xu, X.; Khoo, S. B.; Mok, K. F.; Hor, T. S. A. *J. Chem. Soc., Dalton Trans.* **2000**, 2901.

10.1021/ic011181o CCC: $22.00
Published on Web 11/20/2002

Hg(II). Specifically, we introduced a ferrocene group as an electroactive reference into these heterometallic systems at the functionalized M-site [Pt$_2$(PPh$_3$)$_4$(μ$_3$-S)$_2$HgFc]PF$_6$ (**1**) [Fc = (η^5-C$_5$H$_4$)Fe(η^5-C$_5$H$_5$)] instead of the [Pt$_2$(μ$_2$-S)$_2$] moiety {i.e., [Pt$_2$(μ$_2$-S)$_2$(dppf)$_2$]} in our former Tl compound. Some interesting results were obtained on the electrochemistry of these compounds. We herein report the syntheses and structures of the new functionalized compounds and their electrochemical behaviors, together with the other related Hg(II) and Au(I) compounds synthesized in our previous work. We also carried out a complementary theoretical study that helped us to understand their electronic structures and electrochemical functions.

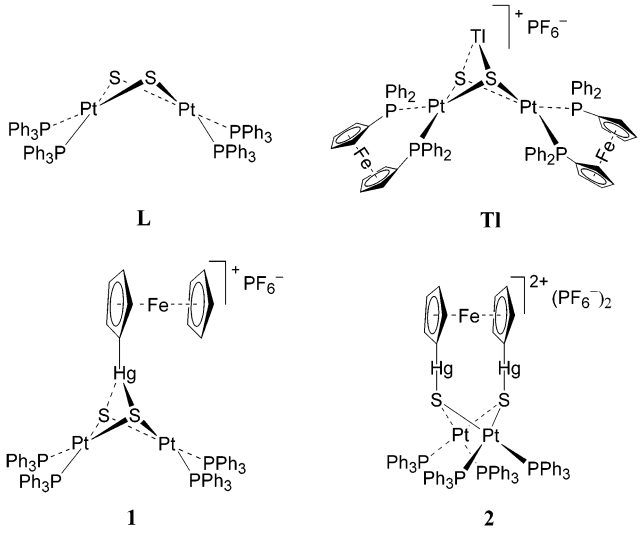

Experimental Section

All solvents were distilled and deoxygenated under argon before use. The starting substrate [Pt$_2$(PPh$_3$)$_2$(μ-S)$_2$] was synthesized from *cis*-[PtCl$_2$(PPh$_3$)$_2$] and Na$_2$S·9H$_2$O;[6] FcHgCl and Fc′(HgCl)$_2$ were synthesized according to the literature method.[7] Other chemicals were used as supplied. Mass spectra were recorded in the positive ion mode using a VG Platform II mass spectrometer. MeOH was used as the mobile phase because of the solubility of the ionic species formed in this solvent. The spectrometer employed a quadrupole mass filter with an *m*/*z* range 0−3 000. The compounds were dissolved in the mobile phase to give a solution typically of approximate concentration 0.1 mmol·L^{-1}, and spectra were recorded for freshly prepared solutions. The dilute sample solution was injected into the spectrometer via a Rheodyne injector fitted with a 10 μL sample loop. A Thermo Separation Products Spectra System P1000 LC pump delivered the solution to the mass spectrometer source (maintained at 60 °C) at a flow rate of 0.02 mL·min^{-1}, and nitrogen was employed as both drying and nebulizing gas. A cone voltage of 20 V was typically used. Confirmation of species was aided by comparison of the observed and predicted isotope distribution patterns. Theoretical isotope distribution patterns were calculated using the Isotope computer program,[8] and species were identified by the *m*/*z* value of the major peak in their respective isotope distribution pattern.

Cyclic voltammetric measurements were performed with an Elchema Model PS-605 potentiostat (Elchema, New York) together with a Model FG-206F Waveform Generator. Voltammograms were recorded with a Graphtec WX-1 100 *x*−*y* recorder (Graphtec Corp., Tokyo, Japan). All experiments were performed in AR grade CH_2Cl_2 that was distilled over P_2O_5 before use. Tetrabutylammonium perchlorate (AR grade, dried for 3 days in a vacuum oven) was used as supporting electrolyte (typically 0.1 M). The concentration of the sample was 1.00×10^{-3} M. The reference electrode was Ag/Ag^+ (0.01 M $AgNO_3$, 0.1 M tetrabutylammonium perchlorate in acetonitrile), and the working electrode was a glassy carbon disk electrode (diameter 3 mm). All experiments were carried out at ambient temperature (25 ± 2 °C).

Synthesis of [Pt$_2$(PPh$_3$)$_4$(μ$_3$-S)$_2$HgFc][PF$_6$] (1) [Fc = (η^5-C$_5$H$_4$)Fe(η^5-C$_5$H$_5$)]. FcHgCl (22.4 mg, 0.0532 mmol) was added to an orange suspension of [Pt$_2$(PPh$_3$)$_4$(μ-S)$_2$] (80.0 mg, 0.0532 mmol) in MeOH (20 mL) in a 100-mL Schlenk tube. The mixture was stirred at 25 °C, initially giving an orange suspension which turned clear orange after ca. 3 h and subsequently, after 24 h, a clear, intensely orange solution. The solution was then filtered through Celite; the filter cake and Celite were washed with MeOH (2 × 5 mL) until the washings were colorless. The pale orange washings and filtrate were combined (30 mL), and excess solid NH_4PF_6 (10 mg, 0.0613 mmol) was added. After stirring for a further 2 h, an orange solid precipitated. Distilled water (10 mL) was then added to the mixture to promote complete precipitation. The orange solid was collected on a fine glass frit, washed successively with distilled water (2 × 10 mL), ethanol (5 mL), and ether (10 mL) and dried in vacuo, affording an orange powder of **1** (95.8%, 88%). Anal. Calcd for $C_{82}H_{69}F_6FeHgP_5Pt_2S_2$: C, 48.42; H, 3.42; P, 7.61; S, 3.15. Found: C, 48.38; H, 3.41; P, 7.56; S, 3.14. ^{1}H NMR (300 MHz, $CDCl_3$): δ_H 7.06−7.34 (m, 60H, 12C$_6H_5$), 4.47 (m, 2H, Cp-H_β), 4.18 (s, 5H, C$_5H_5$), and 4.04 (m, 2H, Cp-H_α). ^{31}P{^{1}H} NMR (121 MHz, $CDCl_3$): δ_P = 20.6 (t, $^1J_{Pt-P}$ = 3017 Hz, 4*P*Ph$_3$), −144.2 (septet, $^1J_{P-F}$ = 713 Hz, PF_6^-).

X-ray Crystal Determination of 1. A suitable orange block crystal (0.18 mm × 0.16 mm × 0.16 mm) was chosen among the crystals obtained by layering hexane over dichloromethane solution of **1** in a refrigerator maintained at 5 °C. A total of 41 604 reflections were collected ($-7 \le h \le 15$, $-16 \le k \le 16$, $-57 \le l \le 52$) in the θ range 1.77−26.37° of which 15 226 were independent (R_{int} = 0.0413) at 223(2) K. The structure was solved by direct methods in conjunction with standard difference Fourier techniques. Non-hydrogen atoms were refined anisotropically. Common isotropic thermal parameters were refined for the solvent atoms. Hydrogen atoms were placed in calculated (d_{C-H} = 0.96 Å) positions. The largest peak and hole in the difference map were 1.036 and −1.972 e Å^{-3}, respectively. The least-squares refinement converged normally with residuals of *R* (based on *F*) = 0.0470, R_w (based on F^2) = 0.0843, and GOF = 1.002 (based upon $I > 2\sigma(I)$). Crystal data for $C_{82}H_{69}F_6FeHgP_5Pt_2S_2$: monoclinic, space group = $P2_1/c$, $z = 4$, a = 12.2184(1) Å, b = 13.3114(2) Å, c = 46.2508(5) Å, β = 94.646(1)°, V = 7497.7(2) Å^3, ρ_{calcd} = 1.802 g cm^{-3}, $F(000)$ = 3926. Crystallographic data of **1** have been deposited with the Cambridge Crystallographic Data Center as supplementary publication no. CCDC-144754. Copies of the data can be obtained, free of charge, on application to CCDC, 12 Union Road, Cambridge CB2 1EZ, U.K. (Fax: (+44) 1223-336-033. E-mail: deposit@ccdc.cam.ac.uk.) A CIF file has been also deposited with ACS as Supporting Information.

(6) Ugo, R.; La Monica, G.; Cenimi, S.; Segre, A.; Conti, F. *J. Chem. Soc. A* **1971**, 522.
(7) Fish, R. W.; Rosenblum, M. *J. Org. Chem.* **1965**, *30*, 1253.
(8) Arnold, L. J. *J. Chem. Educ.* **1992**, *69*, 811.

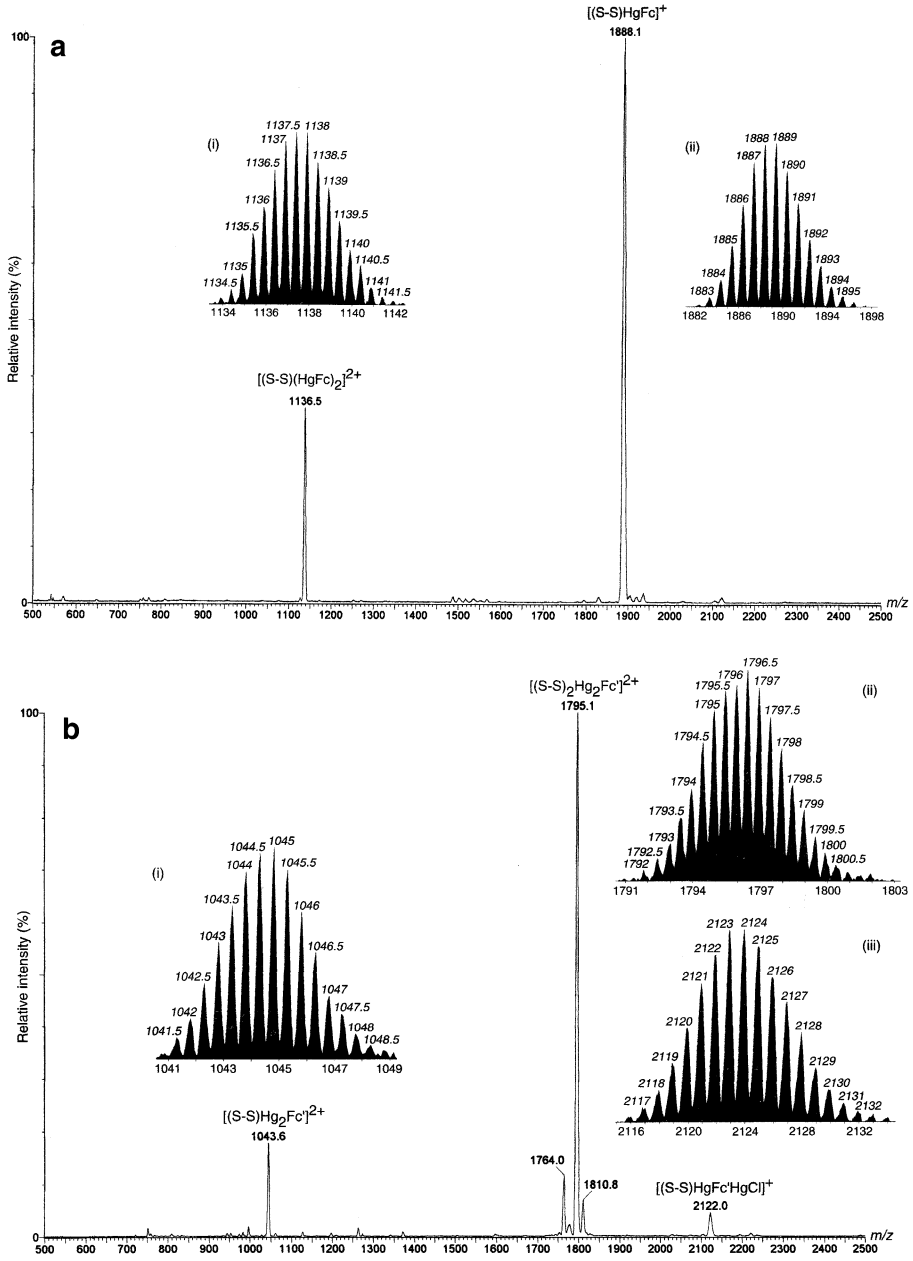

Figure 1. (a) ES mass spectrum of $[Pt_2(\mu_2\text{-}S)_2(PPh_3)_4]$ (**L**) with FcHgCl (cone voltage 20 V). (b) ES mass spectrum of $[Pt_2(\mu_2\text{-}S)_2(PPh_3)_4]$ (**L**) with $Fc'Hg_2Cl_2$ (cone voltage 20 V).

Synthesis of $[Pt_2(PPh_3)_4(\mu_3\text{-}S)_2Hg_2Fc'][PF_6]_2$ (2) [Fc′ = $(\eta^5\text{-}C_5H_4)_2Fe$]. Complex **2** (orange powder, 96 mg, 89%) was obtained using a similar procedure as that of **1** from $Fc'(HgCl)_2$ (34.9 mg, 0.0532 mmol) and $[Pt_2(PPh_3)_4(\mu\text{-}S)_2]$ (80.0 mg, 0.0532 mmol). Anal. Calcd For $C_{82}H_{68}F_{12}FeHg_2P_6Pt_2S_2$: C, 41.41; H, 2.88; P, 7.81; S, 2.70. Found: C, 41.37; H, 2.90; P, 7.79; S, 2.68. ^{1}H NMR (300 MHz, CD_3CN): $\delta_H = 7.32-7.61$ (m, 60H, $12C_6H_5$), 4.68 (m, 4H, Cp-H_β), and 4.33 (m, 4H, Cp-H_α). $^{31}P\{^1H\}$ NMR (121 MHz, CD_3CN): $\delta_P = 22.48$ (t, $^1J_{Pt-P} = 3017$ Hz, 4PPh_3), -142.89 (septet, $^1J_{P-F} = 706$ Hz, PF_6^-).

Computational Details. Density functional theory with a generalized gradient approximation was utilized in all the calculations.[9] The electronic wave functions were expanded in a plane wave basis set, and the ionic cores were described by ultrasoft pseudopotentials.[10] The vacuum region between slabs was over 7 Å. A cutoff energy of 300 eV was used. A convergence check has been performed by increasing the vacuum region to 10 Å and the cutoff energy to 350 eV (the difference in the geometry was found to be below 0.001 Å). All the total energy calculations were performed using CASTEP.[18] The input structures were adopted from the crystal structure directly. For cationic complexes, only the cations were calculated. The output files as CST have been deposited as Supporting Information.

Results and Discussion

Synthesis and Structure. Our recent use of electrospray mass spectrometry (ESMS) demonstrated its value as a combinatorial-like tool in directing syntheses.[11] This results

(9) Perdew, J. P.; Chevary, J. A.; Vosko, S. H.; Jackson, K. A.; Pedeson, M. R.; Singh, D. J.; Fiohais, C. *Phys. Rev. B* **1992**, *46*, 6671.

(10) Vanderbilt, D. *Phys. Rev. B* **1990**, *41*, 7892.

Scheme 1

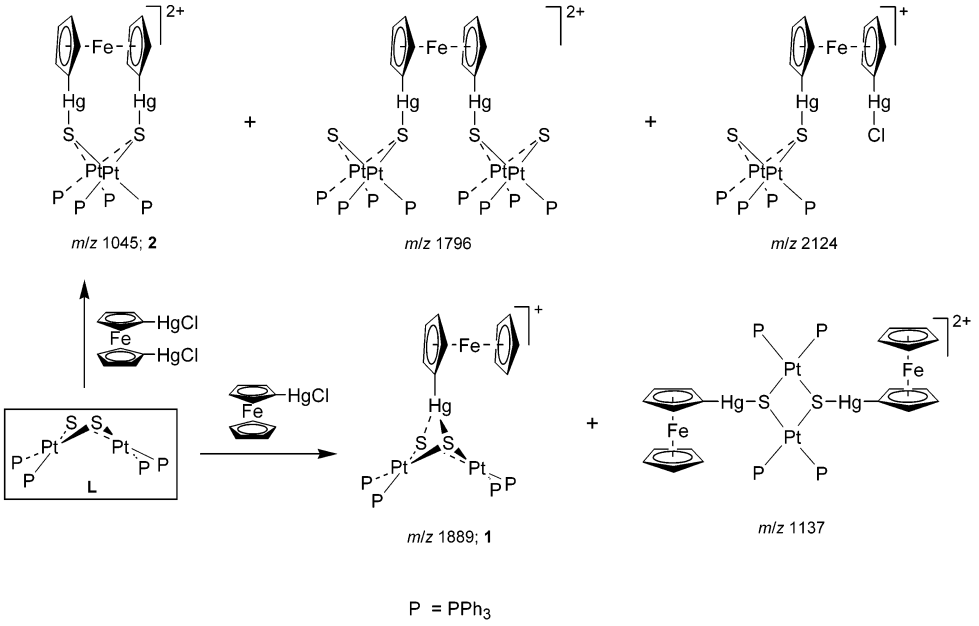

in a procedure that minimizes chemical waste through a predictive approach to the facile synthesis of new heterometallic complexes. A mixture of **L** with FcHgCl gives a clear orange solution with an ES mass spectrum (Figure 1a) which, at a cone voltage of +20 V, shows two peaks at *m*/*z* 1137 and 1889, respectively assigned[8] to the species $[(S-S)(HgFc)_2]^{2+}$ and $[(S-S)HgFc]^+$, where (S−S) = $[Pt_2(PPh_3)_4(\mu\text{-}S)_2]$. With 1 equiv of $Fc'(HgCl)_2$ [Fc′ = $Fe(\eta^5\text{-}C_5H_4)_2$], the ES mass spectrum (Figure 1b) shows, in order of increasing *m*/*z*, a peak assigned as $[(S-S)Hg_2Fc']^{2+}$ (*m*/*z* 1045; 18%), a major peak due to $[(S-S)_2Hg_2Fc']^{2+}$ (*m*/*z* 1796; 100%), and a minor peak from $[(S-S)HgFc'HgCl]^+$ (*m*/*z* 2124; 6%) (Scheme 1). A time-dependent examination of this reaction, in the presence of a slight excess of $Fc'Hg_2Cl_2$, revealed that, over a period of 45 min, the concentration of the $[(S-S)_2Hg_2Fc']^{2+}$ species drops appreciably, yielding predominantly $[(S-S)Hg_2Fc']^{2+}$. The observation of these species, $[(S-S)HgFc]^+$ and $[(S-S)Hg_2Fc']^{2+}$, prompted attempts at their benchtop synthesis. Individual reactions of **L** with stoichiometric amounts of FcHgCl and $Fc'Hg_2Cl_2$[7] followed by metathesis with a slight excess of NH_4PF_6 in methanol gave orange complexes $[Pt_2(PPh_3)_4(\mu_3\text{-}S)_2HgFc][PF_6]$ (**1**) (82%) and $[Pt_2(PPh_3)_4(\mu_3\text{-}S)_2Hg_2Fc'][PF_6]_2$ (**2**) (65%), respectively.

The molecular structure of **1** (Figure 2) shows a triangular $HgPt_2$ core capped on both sides by μ_3-sulfido ligands. Neglecting the metal−metal nonbonding interactions, the d^8 platinum centers exhibit square-planar coordination environments while the mercury(II) center adopts a distorted "T-shaped" geometry, with one Hg−S bond significantly longer (by 26%) than the other [Hg(1)−S(1) 3.0001(18) Å; Hg(1)−

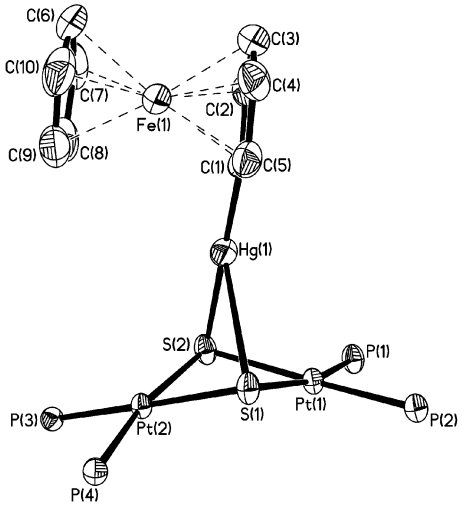

Figure 2. Thermal ellipsoid plot of $[Pt_2(PPh_3)_4(\mu_3\text{-}S)_2HgFc]^+$ (**1**) (anions and phenyl rings of PPh_3 ligands were omitted for clarity).

S(2) 2.381(2) Å] and a near-linear ∠C(1)−Hg−S(2) [179.3(2)°] (see Table 1). Among the $\{Pt_2S_2M\}$ aggregates reported, both "Y-shaped", for example, $[Pt_2(PPh_3)_4(\mu_3\text{-}S)_2Cu(PPh_3)]PF_6$[12] [∠P(3)−Cu(3)−S(1) = 135.7(2)° and ∠P(3)−Cu(3)−S(2) = 139.4(4)°], and T-shaped complexes, for example, $[Pt_2(PPh_3)_4(\mu_3\text{-}S)(\mu_2\text{-}S)HgPh]BPh_4$[11a] [∠C(1)−Hg−S(1) = 113.00(15)° and ∠C(1)−Hg−S(2) = 174.59(16)°] have been identified. Another interesting feature of **1** is the significant disparity between the two Hg···Pt distances (3.067 and 3.340 Å), which is not observed in the isoelectronic gold(I) complexes such as $[Pt_2(PPh_3)_4(\mu_3\text{-}S)_2(AuCl)_2]$[13] [3.111(1) and 3.218(1) Å] and $[Pt_2(PPh_3)_4(\mu_3\text{-}S)(\mu_2\text{-}S)Au(PPh_3)]^+$ [3.314(1) and 3.231(1) Å].[5] The dihedral angle (θ) of the

(11) (a) Fong, S. W. A.; Yap, W. T.; Vittal, J. J.; Hor, T. S. A.; Henderson, W.; Oliver, A. G.; Rickard, C. E. F. *J. Chem. Soc., Dalton Trans.* **2001**, 1986. (b) Fong, S. W. A.; Vittal, J. J.; Henderson, W.; Hor, T. S. A.; Oliver, A. G.; Rickard, C. E. F. *Chem. Commun.* **2001**, 421. (c) Yeo, J. S. L.; Vittal, J. J.; Henderson W.; Hor, T. S. A. *J. Chem. Soc., Dalton Trans.* **2001**, 315.

(12) Liu, H.; Tan, A. L.; Xu, Y.; Mok, K. F.; Hor, T. S. A. *Polyhedron* **1997**, *16*, 377.

(13) Bos, W.; Bour, J. J.; Schlebos, P. P. J.; Hageman, P.; Bosman, W. P.; Smits, J. M. M.; van Wietmarschen, J. A. C.; Beurskens, P. T. *Inorg. Chim. Acta* **1986**, *119*, 141.

Table 1. Selected Bond Distances (Å) and Bond Angles (deg) for Compound **1**

Bond Distances			Bond Angles		
Hg(1)−C(1)	2.062(9)	C(1)−Hg(1)−S(2)	179.3(2)	P(3)−Pt(2)−P(4)	99.78(7)
Hg(1)−S(1)	3.001(19)	C(1)−Hg(1)−S(1)	110.1(2)	S(2)−Pt(1)−S(1)	81.76(6)
Hg(1)−S(2)	2.381(2)	S(2)−Hg(1)−S(1)	69.20(6)	S(2)−Pt(2)−S(1)	82.26(6)
Pt(1)−S(1)	2.3332(18)	C(1)−Hg(1)−Pt(1)	129.0(2)	Pt(2)−S(1)−Pt(1)	93.96(7)
Pt(1)−S(2)	2.3996(18)	S(2)−Hg(1)−Pt(1)	50.36(4)	Pt(2)−S(2)−Pt(1)	91.66(6)
Pt(2)−S(1)	2.3428(18)	S(1)−Hg(1)−Pt(1)	45.22(4)	Hg(1)−S(1)−Pt(1)	68.90(5)
Pt(2)−S(2)	2.3666(18)	C(1)−Hg(1)−Pt(2)	134.6(2)	Hg(1)−S(2)−Pt(1)	91.66(6)
Pt(1)−P(1)	2.3156(19)	S(2)−Hg(1)−Pt(2)	45.11(4)	Hg(1)−S(1)−Pt(2)	76.29(5)
Pt(1)−P(2)	2.2735(19)	S(1)−Hg(1)−Pt(2)	42.95(3)	Hg(1)−S(2)−Pt(2)	89.44(7)
Pt(2)−P(3)	2.2928(18)	Pt(1)−Hg(1)−Pt(2)	64.330(9)		
Pt(2)−P(4)	2.2936(18)	P(2)−Pt(1)−P(1)	100.76(7)		

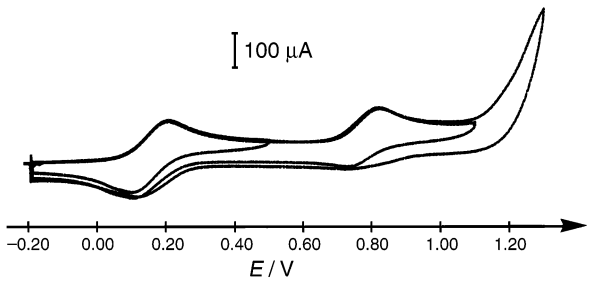

Figure 3. Anodic scan of $[Pt_2(PPh_3)_4(\mu_3\text{-}S)_2HgFc][PF_6]$ (**1**) between −0.20 and +1.10 V in CH_2Cl_2.

$\{Pt_2S_2\}$ butterfly core along the S(1)···S(2) axis is 147.4°. The two μ-sulfur atoms bind to the heterometal Hg at a chelating angle of 69.20(6)°. These examples suggest that, although **L** is primarily a chelating ligand, it has an inherent flexibility to support a range of metals with different coordination and geometric demands.

Electrochemistry. Cyclic voltammetry is used to study the electrochemical behavior of these aggregates. Dichloromethane is used as solvent in all the electrochemical experiments because of good solubility of these compounds. In **1**, there are two discrete, reversible waves at the anodic end between −0.20 to +1.10 V (Figure 3). The first reversible wave at $E^{o\prime} = +0.15$ V is assigned to the ferrocene/ferrocenium couple (Fc/Fc^+) attached to the Hg(II) center (cf. +0.35 V for free ferrocene under similar experimental conditions). The second oxidation revealed a slight degree of decay of the oxidized product upon reversal such that $i_{pc}/i_{pa} \approx 0.6$; the respective oxidation and reduction peaks for this second process are $E_{p,a} = +0.82$ V and $E_{p,c} = +0.74$ V ($\Delta E_p = 80$ mV). This second oxidation likely corresponds to a one-electron-transfer process as evidenced by comparison of its peak current with that of the Fc/Fc^+ peak. These two peaks remain reproducible as long as the oxidative scanning did not exceed the +1.10 V mark. Analogous anodic scanning of complex **2** revealed only one peak at $E^{o\prime} = +0.26$ V, assigned to the Fc/Fc^+ couple. This peak is slightly shifted to a higher potential compared to **1**. Cathodic scanning of complex **1** revealed only one irreversible peak at −1.91 V, which is near the background breakdown, while two irreversible peaks are observed in **2** (at −1.49 and −1.80 V). Unlike the mercury−phosphine complexes $[Pt_2(PPh_3)_4(\mu_3\text{-}S)_2HgPPh_3](PF_6)_2$ and $[Pt_2(PPh_3)_4(\mu_3\text{-}S)_2Hg_2(\mu_2\text{-}Cl)_2(PPh_3)_2](PF_6)_2$ reported earlier,[5] scanning both **1** and **2** between −2.40 and +1.00 V did not reveal any sharp peaks attributable to the reduction of Hg(II) to Hg(0) and subsequent stripping of the Hg(0) from the electrode surface.

Initial studies of complexes **1** and **2** by anodic scanning up to +1.60 V in CH_2Cl_2 also indicated that a surface film was formed. The results will be reported subsequently.

To compare the electrochemical properties of these two compounds with the related complexes $[Pt_2(PPh_3)_4(\mu_3\text{-}S)_2HgPPh_3](PF_6)_2$ (**3**),[5] $[Pt_2(PPh_3)_4(\mu_2\text{-}S)(\mu_3\text{-}S)HgPh]PF_6$ (**4**),[11a] and $[Pt_2(PPh_3)_4(\mu_2\text{-}S)(\mu_3\text{-}S)AuPPh_3]PF_6$ (**5**)[14] (the crystal data of all these compounds have been reported; see accompanying graphic here for their structures), we carried out the electrochemical studies of compounds **3**, **4**, and **5**, which were synthesized and purified similarly as reported.[5,11a]

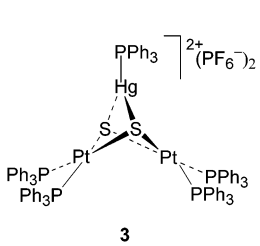

3

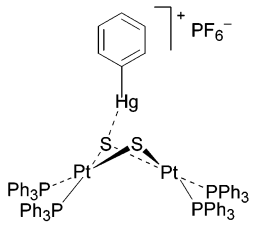

4

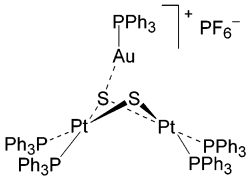

5

The electrochemistry of **3** has been reported in our previous paper, in which a reversible peak occurs at redox potential $E^{o\prime} = +1.05$ V (Figure 4a).[5] It shows a near-reversible one-electron-transfer oxidation with $E_{p,a} = 1.10$ V and $E_{p,c} = 1.01$ V ($\Delta E = 90$ mV). The $i_{p,c}/i_{p,a}$ ratio is about 0.7, with some post-oxidation product decay. When PPh_3 on Hg(II) (in **3**) is replaced by Ph (in **4**), one irreversible peak was observed at $E_p = +0.73$ V upon anodic scan. When Hg(II) (in **3**) is replaced by Au(I) (in **5**), one reversible redox process was also found in its cyclic voltammogram, but a fairly large potential shift ($E^{o\prime} = +0.32$ V**)** is registered [Figure 4b]. It is also a near-reversible oxidation with $E_{p,a} = 0.36$ V and $E_{p,c} = 0.28$ V ($\Delta E = 90$ mV). The $i_{p,c}/i_{p,a}$ ratio is about 0.7. This one-electron-transfer is also verified

(14) Li, Z.; Loh, Z.-H.; Mok, K. F.; Hor, T. S. A. *Inorg. Chem.* **2000**, 5299.

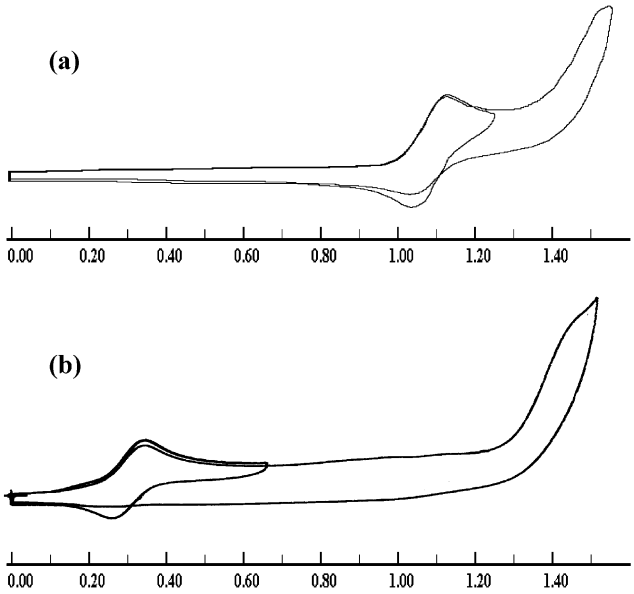

Figure 4. Cyclic voltammograms of **3** and **5**. (a) Anodic scan from 0.0 to 1.50 V of compound **3** (50 mV/sec) in CH_2Cl_2. (b) Anodic scan from 0.0 to 1.50 V of compound **5** (scan rate 100 mV/sec) in CH_2Cl_2.

Table 2. Electrochemical Data for the Compounds

cmpd	$E^{\circ\prime}_{(0/+)}$(R) or $E_{p,(0/+)}$(IR) (V)[a]	ΔE_p (mV)	$E^{\circ\prime}_{(+1/+2)}$ (V)	ΔE_p (mV)	possible oxidation sites
1	+0.15 (R)	80	+0.78	80	Fe(II)−Fe(III) S(−II)−S(−I)
2	+0.26 (R)	80			
3	+1.05 (R)	90			S(−II)−S(−I)
4	+0.73 (IR)				S(−II)−S(−I)
5	+0.32 (R)	90			Pt(II)Pt(II)− Pt(III)Pt(II)

[a] R = reversible; IR = irreversible.

by comparing the current of these compounds at the same concentration. The cyclic voltammogram data are summarized in Table 2.

Theoretical Studies. The electrochemical results raise some pertinent questions on these sulfido aggegates. First, it is readily understood that in compound **1** the first oxidation peak is the oxidation of Fe(II) on the Fc fragment. However, it is not clear which oxidation process corresponds to the second peak. Second, the nature of the oxidation, as found in the CV diagram of **3**, **4**, and **5**, is not obvious. Third, it is unclear why the oxidation potential of compound **5** is much lower than those of the other compounds. Fourth, these complexes are related closely in terms of structures, ligand behavior, and isoelectronic character, yet their CV profiles are different and, to a large extent, unpredictable. Why?

To answer these questions, DFT calculations have been carried out on compounds **1**, **3**, **4**, **5**, and the free ligand **L** using the CASTEP program.[15] Their authenticated X-ray crystal structures, except for the PPh_3 groups being replaced by PH_3 in all the systems, were used as models for the calculations. Optimized geometries are listed in Table 3, together with the experimental data for comparison. It shows that all the calculated structures agree well with the

(15) Payne, M. C.; Teter, M. P.; Allan, D. C.; Arias, T. A.; Joannopoulos, J. D. *Rev. Mod. Phys.* **1992**, *64*, 1045.

Table 3. Bond Length (Å) Comparisons of the Optimized output Structures and Crystal Structures of **1**, $\mathbf{1}^{2+}$, **3**, **4**, and **5**

	1	$\mathbf{1}^{2+}$	**3**	**4**	**5**
Hg−S_2 or Au−S_2	2.381(2)[a] (2.449)[b]	2.425	2.428(2) (2.469)	2.4079(12) (2.464)	2.338(2) (2.355)
Hg−S_1 or Au−S_1	3.0001(19) (3.236)	3.123	2.694(2) (2.654)	2.9286(12) (3.076)	3.134(2) (3.113)
Pt_1−S_2	2.3666(18) (2.389)	2.396	2.386(2) (2.389)	2.3684(11) (2.379)	2.360(2) (2.369)
Pt_1−S_1	2.3428(18) (2.338)	2.300	2.386(2) (2.382)	2.3560(11) (2.347)	2.337(2) (2.347)
Pt_2−S_2	2.3996(18) (2.399)	2.406	2.423(2) (2.397)	2.4074(11) (2.388)	2.379(2) (2.391)
Pt_2−S_1	2.332(18) (2.349)	2.311	2.360(2) (2.377)	2.3461(11) (2.361)	2.356(2) (2.351)
Hg−P_5 or Au−P			2.402(2) (2.406)		2.252(2) (2.227)
Pt_1−Pt_2	3.419 (3.393)	2.377	3.306 (3.270)	3.268 (3.220)	3.390 (3.311)
S_1−S_2	3.098 (3.164)	3.087	3.144 (3.168)	3.122 (3.167)	3.075 (3.150)
Hg−C	2.062(9) (2.059)	2.075		2.081(5) (2.090)	

[a] From crystal structure. [b] From optimized structure.

experimental results. It is known that the HOMO plays a key role in governing the electrochemical activity. Therefore, we concentrate on the frontier orbitals in these compounds. Important isosurfaces of electron density in frontier orbitals are shown in Figure 5.

As expected, the HOMO of **1** contains strong d orbital character located on the ferrocenyl Fe(II) atom (in Figure 5a). This implies that the first oxidation peak arises from the loss of one electron from this Fe(II) d orbital, which is consistent with the observed redox potential ($E^{\circ\prime} = +0.15$ V). It is slightly lower than that of the free ferrocene in the same solvent ($E^{\circ\prime} = +0.35$ V) because the ferrocenyl fragment is negatively charged. The second reversible oxidation peak is at $E = +0.78$ V. To identify the element responsible for this peak, we calculated $\mathbf{1}^{2+}$, viz. the two-electron oxidation product of **1**. We found that the LUMO of $\mathbf{1}^{2+}$ locates on a p orbital of S1(−II) and a d orbital of the Fe atom (in Figure 5b). This indicates that, in the two-step oxidation process, the two electrons are removed from Fe and S1. This suggests that S1 is the second oxidation center. This is reasonable because Fe(III) is unlikely to be further oxidized. Structural comparisons between **1** and $\mathbf{1}^{2+}$ show that large changes of bond lengths are among the 10 Fe−C bonds and the 2 S1−Pt bonds. This also supports the electron loss in these areas. It is reasonable that the second peak in **1** does not appear in **2** because after one-electron oxidation **1** is doubly positively charged while **2** is triply positively charged.

It is interesting to relate the redox states of compounds **3**, **4**, and **5** to the frontier orbitals of free ligand **L**. The CV data of **L** could not be obtained because of its poor solubility in acceptable solvents. Its frontier orbitals are located on the two sulfur and two platinum atoms, that is, the $\{Pt_2S_2\}$ core. The first five highest occupied molecular orbitals consist mainly of p orbitals of the sulfur, followed by the orbitals containing mainly d orbital character of Pt atoms. This electronic feature is consistent with the strong Lewis basic

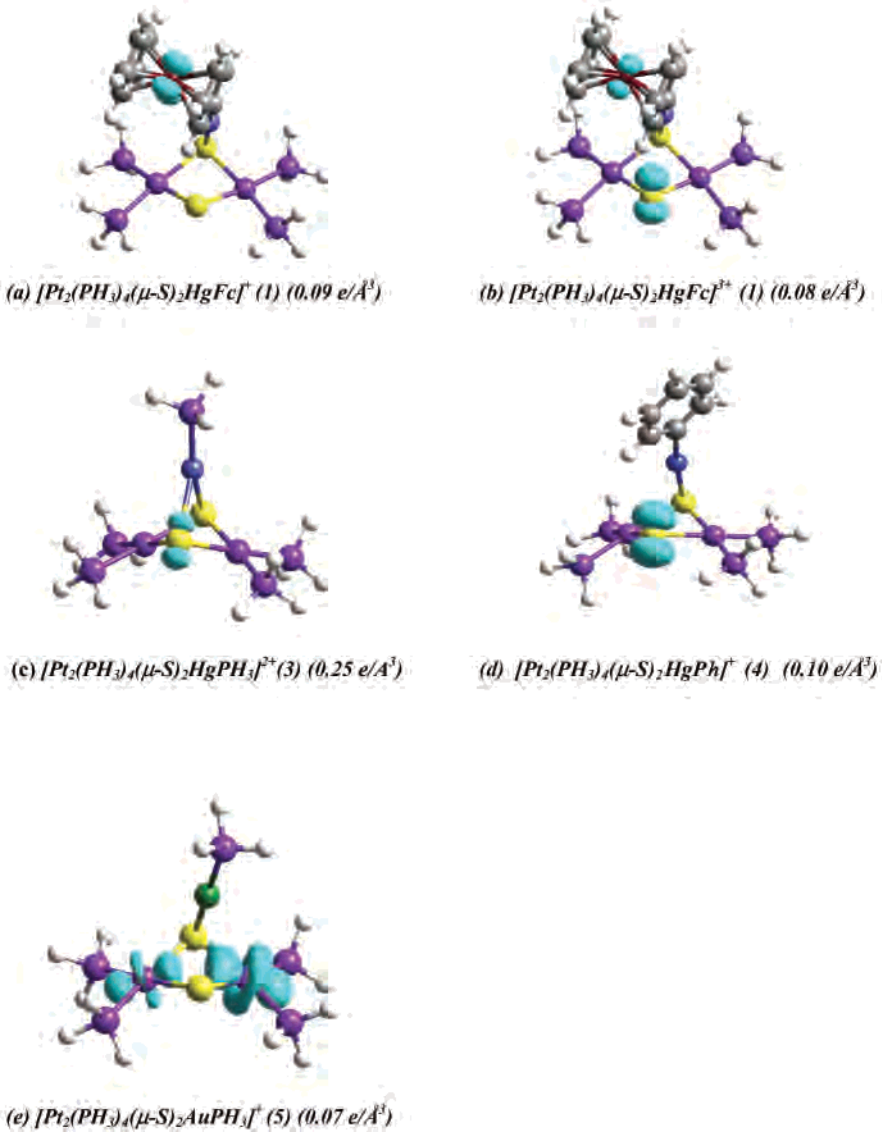

Figure 5. Electron density isosurface plot of the HOMO orbitals (a, c, d, e) and LUMO orbital (b) (electron density is shown in the bracket).

character of the sulfide centers of **L**, and hence its rich metalloligand chemistry.

For compounds **3** and **4**, the HOMO orbitals (shown in Figure 5c,d, respectively) are very similar to those in **L**. This suggests that the one-electron oxidation process observed in the CV of **3** and **4**, similar to the second peak of compound **1**, is a ligand-based process involving electron removal from mainly the p orbital of the S1(−II) which has a longer Hg−S bond distance than S2(−II). Although coordinated sulfide is generally not perceived as an oxidation center, the possibility of the HOMO orbital of bridging S(−II) as an electron source has been discussed by Zanello and co-workers on the CV of the 1,1′-ferrocene dichalcogenido complexes of rhodium and iridium.[16] It is reasonable that the oxidation potential of **3** is higher than that of **4** because **3** is doubly positively charged and **4** is singly positively charged. It is also interesting to note that there is a correlation between the redox potential of the Hg compounds and their HOMO energies [**1**, −3.62 eV (the energy level of HOMO), +0.15 V (the redox potential upon anodic scan); **3**, −6.33 eV, +1.05 V; **4**, −4.82 eV, +0.73 V].

Compound **5**, the analogue of compound **3**, has a completely different HOMO orbital, shown in Figure 5e. It is delocalized on d orbitals of the two Pt atoms rather than on the two S atoms. As a result, the two Pt(II) atoms are the redox center. This explains the significant difference between the CV profile of **5** compared to **3** and **4**. This fundamental difference is reflected in the unique electrochemical behavior of **5**. Its reversible oxidative peak ($E^{\circ\prime}$ = 0.32 V) shifts significantly from those of **3** ($E^{\circ\prime}$ = 1.05 V), **1** ($E^{\circ\prime}$ = 0.78 V), and **4** (E_p = 0.73 V).

Naturally, one may ask why compound **5** is unique. To understand this, we analyzed the electronic structures of **5** and its isoelectronic analogue, **3**. It shows that the major difference in the frontier orbitals between **3** and **5** lies at the p orbitals of S atoms. In **3**, the HOMO contains a strong S p orbital character while in **5** the orbitals comprising mainly the p orbital characters of S are located at lower energy

(16) Zanello, P.; Casarin, M.; Pardi, L.; Herberhold, M.; Jin, G.-X. *J. Organomet. Chem.* **1995**, *503*, 243.

levels. This may be caused by the stronger bonding interaction between Au(I) and S(−II) compared to that of Hg(II) and S(−II). The strong interaction of Au(I) and S(−II) significantly stabilizes (and pushes lower) the S(p)−Au(d) bonding orbitals of **5**, while the energy level of the S(p) orbitals in the Hg−S complex is considered "normal". This analysis is consistent with the following observations: (i) the bond energy of Au(I)−S is about two times larger than that of Hg(II)−S,[17] and (ii) the d orbital level of Au(I) is significantly higher than that of Hg(II). This suggests that the binding metals on ligand **L** may alter the electronic structure and bring in significant changes in the properties of the corresponding {Pt_2S_2M} aggregates.

It is worth mentioning that our calculations model molecules in the gas phase, which may be different from the solution experiments, because in the calculations (i) the solvent effect is omitted; (ii) the interaction between the molecules and the electrolytes is neglected; and (iii) the interactions between the electrodes and the molecules are not considered. Although these issues are complicated and beyond the current scope of DFT calculations, our calculations nevertheless gave some useful insights in the chemistry here.

Conclusion

For the first time in this series of heterometallic aggregates, we have identified, unexpectedly, a ligand (sulfide)-based oxidation process. This oxidation adds a new dimension to the expected redox activities of the metals and the ferrocenyl moieties in these architectures. It also demonstrated the value of sulfide, not only as a stabilizing capping ligand but also as an electron transfer mediator within the multimetallic framework. The high stability of many of these aggregates and clusters could be attributed, at least partly, to the ability of sulfide to leverage such a property to dissipate excess charge from one metal to another. Different electrochemical behaviors of these compounds can be rationalized using DFT calculations. The interplay of these atoms on the {Pt_2S_2M} core holds the key to the design of a particular material with a predetermined set of properties and functions. Using a building block approach to molecular assembly and a combination of structural, electrochemical, and theoretical techniques, we have established an important structure/activity relationship in these multi-intermetallic sulfide materials.

Acknowledgment. The authors acknowledge the National University of Singapore (NUS) for financial support. X.X. thanks NUS for a postdoctoral fellowship. S.-W.A.F., Z.L., and F.Z. thank NUS for research scholarship awards. Technical support from the Department of Chemistry of NUS is appreciated.

Supporting Information Available: Crystallographic data in CIF format. CST files in text format from the DFT calculation. This material is available free of charge via the Internet at http://pubs.acs.org.

IC011181O

(17) Weast, R. C. *Handbook of Chemistry and Physics*, 56th edition, CRC Press, Cleveland, 1975.
(18) CASTEP 4.2 Academic version, licensed under the UKCP-MSI Agreement, 1999. *Rev. Mod. Phys.* **1992**, *64*, 1045.